Mechanical Testing and Diagnosis
ISSN 2247 – 9635, 2017 (VII), Volume 1, pp. 5-15

SIMULATION OF AN AXISYMMETRICAL COANDA PROFILE WITH RADIAL CLEARANCE

Sorin Gabriel CONSTANTINESCU[*], Mihai NICULESCU[**], Lorena DELEANU[*]

[*] "Dunarea de Jos" University of Galati, Galati, Romania
[**] INCAS, Romania

Corresponding author: Sorin Gabriel CONSTANTINESCU, e-mail: sorin.g.constantinescu@gmail.com

ABSTRACT

This paper presents the results of simulating the air flow as jet attached to a Coanda profile. The simulation on a Reynolds Averaged Navier-Stokes (RANS) model based on the concept of turbulent viscosity could give valuable information on the behavior of such a system if the appropriate limit and material conditions are imposed by the designers. The model proposed by the authors could simulate with sufficient accuracy the process of jet attaching on the Coanda profile. The jet is accelerated across the upside of the Coanda airfoil and, as a consequence of Bernoulli's law, the static pressure drops and for thinner jets and higher velocities, the jet does not detach from the surface of the Coanda airfoil.

Keywords: radial clearance, Coanda profile, CFD model, axisymmetric flow, jet attaching

1. INTRODUCTION

Unfortunately, existing research about the flow of gas jets partially limited by a surface with curved profile [1], [2], [3] or the flow of gas into Coanda nozzles, only refers to straight flows [4]. Radial jets limited by a curved surface are practically not studied at all. The mechanics of radial jet attachment to a curved surface are not clear, and the way in which the geometrical parameters of the nozzle and the flow dynamics influence the size of the aerodynamical forces created by the Coanda nozzle or profile is not deeply studied. The specialized literature clearly highlights that the increase in the radial jet flow speed leads to an increase of the lift force.

As a result of documentation analysis, the elaboration of a model facilitates the selection of parameters for a laboratory study, which allows for a flow simulation for radial jets produced by Coanda nozzles (profiles), in order to establish the influence of certain geometrical parameters of the studied nozzle, for high flow speeds.

2. THEORETICAL BACKGROUND

The closing of the Navier-Stokes mediated Reynolds equations system requires the modeling of the Reynolds tensions $-\left\langle \rho u'_i u'_j \right\rangle$ which are used in the impulse and turbulent heat flux equations and $-\left\langle \rho u'_j H' \right\rangle$, which are used in the energy equation, through a turbulence model [5]. Currently, there is no turbulence model acceptable for any turbulent movement, because all known models present limits, which narrow the range of their applicability domain [6], [7]. Consequently, there are turbulence models with zero differential equations (also called algebric models, which are not used anymore), models with one and with two equations (which are the most used, presently) and so on. To note that the most complex

model is comprised of 12 differential equations with partial derivatives [8], [9].

Inside a turbulent boundary layer, there are 2 distinct areas:

- an area further away from the wall (external area), which is controlled by the turbulence,
- an area close to the wall (internal area), which is controlled by the viscosity.

This differentiation of areas comes right from the analysis of experimental data, which refer to the total tension in the fluid. It has been found that the total tension τ_{eff} is practically given by the turbulent component $-\left\langle \rho u'_i u'_j \right\rangle$ on almost the entire thickness of the boundary layer (approx. 90%), with the exception of a small adjacency of the wall, where the molecular viscosity becomes predominant.

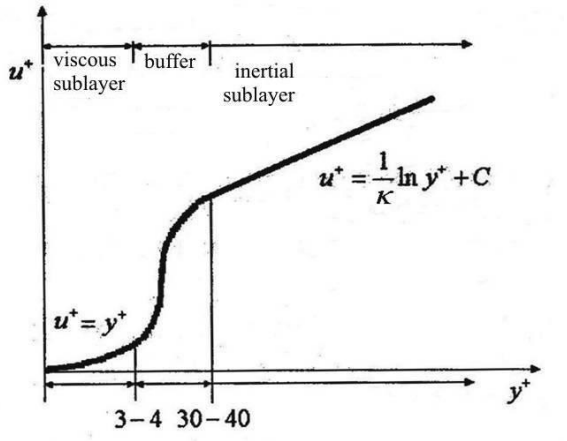

Fig. 1. At wall law [12]

In the internal area (Fig. 1), there are three zones that can be highlighted [10], [11], [12]:

1) the viscous sublayer, in which the speed variation law is considered to be universal: $u^+ = y^+$ where

$$u^+ = \frac{u}{u_\tau}, \tag{1}$$

$$y^+ = \frac{u_\tau y}{\nu} \tag{2}$$

the friction speed u_τ is defined by the following relation:

$$u_\tau = \sqrt{\frac{\tau_P}{\rho}}, \tag{3}$$

and τ_P represents the wall friction effort.

The viscous sublayer, also sometimes incorrectly called laminar sublayer (due to the presence of speed fluctuations), covers the area from the wall to $y^+ \approx 4(5)$.

2) the inertial (or logarithmic) sublayer, which is also distinguished by a universal speed distribution law (also called logarithmic law or at wall law) $u^+ = \frac{1}{\kappa}\ln y^+ + C$, where $\kappa \approx 0.41$ is the constant of Von Kármán and C is a universal constant with the value of about 5.25 [12]. Experiments show that the logarithmic law is valid for a wide variety of conditions, like high pressure gradient flows (in the case of adverse pressure gradient, up to the adjacency of the separation point) or turbulent flows with low Reynolds numbers. The experiments show that the at wall law is verified for $y^+ \geq 40$ [10].

3) the buffer sublayer, which develops between the viscous sublayer and the inertial sublayer, therefore corresponding to the interval $5 < y^+ < 40$.

Boussinesq has proposed for the apparent (turbulent) tensions to be expressed according to the mean deformation speeds through an apparent (turbulent) viscosity:

$$-\rho\left\langle u'_i u'_j \right\rangle + \frac{2}{3}k\delta_{ij} = \mu_t\left(\frac{\partial u_i}{\partial x_j} + \frac{\partial u_j}{\partial x_i} - \frac{2}{3}\frac{\partial u_k}{\partial x_k}\delta_{ij}\right) \tag{4}$$

In the case of the boundary layer, the Boussinesq hypothesis becomes:

$$-\rho\left\langle u'v' \right\rangle = \mu_t \frac{\partial u}{\partial y} \tag{5}$$

The Boussinesq hypothesis is based on the analogy between the impulse transport through the turbulent agitation and the molecular agitation, even though this analogy is not justified because the molecular agitation is independent from the movement and also exists in static fluids, while the turbulent fluctuations are intrinsically linked with the movement. The major disadvantage of the Boussinesq hypothesis consists in the assumption that turbulent viscosity is an isotropic scalar quantity, a fact which is not very true, especially for the flows with strong vertices, secondary flows etc.

By direct analogy with the turbulent impulse transport, the turbulent thermic flux can be expressed according to the temperature gradient:

$$-\rho\left\langle u'_j T' \right\rangle = \rho\alpha_t \frac{\partial T}{\partial x_j} \tag{6}$$

where α_t is the turbulent thermic diffusion coefficient. The Reynolds analogy between the impulse transport and the heat transport implies the

existence of a connection between the apparent thermic diffusivity α_t and the turbulent viscosity μ_t through a relation such as:

$$\alpha_t = \frac{\nu_t}{\mathrm{Pr}_t} = \frac{\mu_t / \rho}{\mathrm{Pr}_t} \tag{7}$$

where Pr_t is the turbulent Prandtl number, which is usually considered constant. Recently conducted research has highlighted a variation of the turbulent Prandtl number over the boundary layer's thickness, so more exact calculations are currently undergoing, discarding the hypothesis of the constant turbulent Prandtl number [10].

On the criteria of using the Boussinesq hypothesis, two categories of turbulence models can be highlighted:

- models with apparent viscosity (which use the Boussinesq hypothesis) and
- models with transport equations for the Reynolds tensions, which do not employ the concept of apparent viscosity.

The turbulence model developed by Spalart and Allmaras [13] has only one transport equation for the modified cinematic turbulent viscosity. Spalart and Allmaras started from the k-ε model, which is the most popular turbulence model with 2 equations. The standard k-ε turbulence model (just as it was created by Jones and Launder [10]) has two main disadvantages:

- it is much too dissipative (it over evaluates the turbulent viscosity μ_t),
- it is a turbulence model only for high Reynolds numbers, in other words, the viscous sublayer and the transition sublayer between the viscous one and the inertial (logarithmic) one, cannot be calculated and, therefore, imply the use of wall functions, which represent with considerable error the detachment and reattachment of the boundary layer to the wall, due to the simplificating hypothesis that they employ.

Starting from the k-ε turbulence model, Spalart and Allmaras have created a new turbulence model, which is relatively simple, with only one transport equation that removes the two major disadvantages stated above.

The standard k-ε turbulence model [14] is valid only for the completely developed turbulence area and, therefore, cannot be applied in the viscous sublayer or the transition sublayer between the viscous one and the inertial one. Consequently, the limit conditions for the transport equations of this turbulence model cannot be imposed at the wall. Let P be a point located at y_P distance from the wall, where the speed parallel to the wall is u_P (Fig. 2). The P point is presumed to be located far enough from the wall for it to belong to the inertial area of the boundary layer, where the logarithmic law is valid as long as there is no flow detachment:

$$\frac{u_P}{u_\tau} = \frac{1}{\kappa} \ln \frac{u_\tau y_P}{\nu} + C \tag{8}$$

which allows for the determination of the u_τ friction speed through a numerical method (for instance, the secant method or Newton–Raphson). Using the hypothesis of local equilibrium between the generation of turbulent kinetic energy G_k and the turbulent dissipation ε at point P, $G_{k_P} = \varepsilon_P$, the following relations can be deduced:

$$k_P = \frac{u_\tau^2}{\sqrt{C_\mu}}, \tag{9}$$

$$\varepsilon_P = \frac{u_\tau^3}{\kappa y_P} \tag{10}$$

which will be considered as limit conditions for the inertial (logarithmic) area of the boundary layer (Fig. 2).

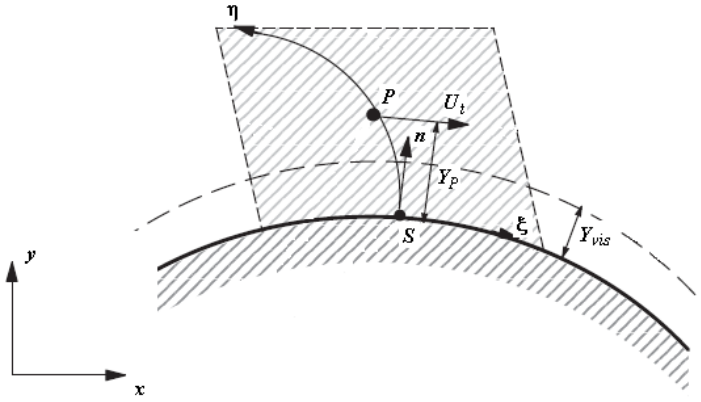

Fig. 2. Imposing the limit conditions in the inertial area [12]

Some CFD codes (for example, Fluent) solve the transport equation for the turbulent kinetic energy k up to the wall, where the condition $k_P = 0$ is imposed.

Using the logarithmic law and the hypothesis of local equilibrium between the generation of turbulent kinetic energy G_k and the turbulent dissipation ε at point P, the following relation can be deduced:

$$\varepsilon_P = \frac{C_\mu^{3/4} k_P^{3/2}}{\kappa y_P} \tag{11}$$

The SST k-ω turbulence model was developed by Menter [20] with the purpose of combining the advantages of the k-ω and k-ε turbulence models. The transport equations of the SST k-ω turbulence model are similar to those of the k-ω turbulence model:

$$\frac{\partial}{\partial t}(\rho k) + \frac{\partial}{\partial x_i}(\rho k u_i) = \frac{\partial}{\partial x_j}\left(\Gamma_k \frac{\partial k}{\partial x_j}\right) + G_k - Y_k \tag{12}$$

$$\frac{\partial}{\partial t}(\rho\omega) + \frac{\partial}{\partial x_i}(\rho\omega u_i) = = \frac{\partial}{\partial x_j}\left(\Gamma_\omega \frac{\partial \omega}{\partial x_j}\right) + G_\omega - Y_\omega + D_\omega \tag{13}$$

The diffusivities for the SST k-ω turbulence model are given by the following relations:

$$\Gamma_k = \mu + \frac{\mu_t}{\sigma_k} \tag{14}$$

and

$$\Gamma_\omega = \mu + \frac{\mu_t}{\sigma_\omega} \tag{15}$$

where σ_k şi σ_ω are the turbulent Prandtl numbers associated with the turbulent kinetic energy k and its specific dissipation ω:

$$\sigma_k = \frac{1}{\frac{F_1}{\sigma_{k,1}} + \frac{1-F_1}{\sigma_{k,2}}} \tag{16}$$

and

$$\sigma_\omega = \frac{1}{\frac{F_1}{\sigma_{\omega,1}} + \frac{1-F_1}{\sigma_{\omega,2}}} \tag{17}$$

The fixed values for this turbulence model $\sigma_{k,1}$, $\sigma_{k,2}$, $\sigma_{\omega,1}$ and $\sigma_{\omega,2}$ are: $\sigma_{k,1} = 1.176$, $\sigma_{k,2} = 1.0$, $\sigma_{\omega,1} = 2.0$, $\sigma_{\omega,2} = 1.168$, while the F_1 and Φ_1 functions are given by the following relations:

$$F_1 = \tanh\left(\Phi_1^4\right) \tag{18}$$

$$\Phi_1 = \min\left[\max\left(\frac{\sqrt{k}}{0.09\omega y_P}, \frac{500\mu}{\rho y_P^2 \omega}\right), \frac{4\rho k}{\sigma_{\omega,2} D_\omega^+ y^2}\right] \tag{19}$$

where y_P is the distance to the closest wall and D_ω^+ is the positive section of the transverse diffusion expression:

$$D_\omega^+ = \max\left[2\rho \frac{1}{\sigma_{\omega,2}} \frac{1}{\omega} \frac{\partial k}{\partial x_j} \frac{\partial \omega}{\partial x_j},\ 10^{-20}\right] \tag{20}$$

The turbulent diffusion μt can be obtained from the relation:

$$\mu_t = \frac{\rho k}{\omega} \frac{1}{\max\left[\frac{1}{\alpha^*}, \frac{\Omega F_2}{a_1 \omega}\right]} \tag{21}$$

where:

$$\Omega = \sqrt{2\Omega_{ij}\Omega_{ij}}, \tag{22}$$

$$\Omega_{ij} = \frac{1}{2}\left(\frac{\partial u_i}{\partial x_j} - \frac{\partial u_j}{\partial x_i}\right), \tag{23}$$

$$F_2 = \tanh\left(\Phi_2^2\right), \tag{24}$$

$$\Phi_2 = \max\left[2\frac{\sqrt{k}}{0.09\omega y_P}, \frac{500\mu}{\rho y_P^2 \omega}\right], \tag{25}$$

$$a_1 = 0.31 \tag{26}$$

Inside of the transport equation ρk, G_k represents the generation of turbulent kinetic energy k and is defined by the following relation:

$$G_k = \min\left(G_k, 10\rho\beta^* k\omega\right) \tag{27}$$

where G_k represents the generation of turbulent kinetic energy k, calculated in the same way as for the standard k-ω [31] turbulence model:

$$G_k = \mu_t S^2 \tag{28}$$

where the module of the S tensor is defined in the same way as for the standard k-ε turbulence model:

$$S = \sqrt{2S_{ij}S_{ij}} \tag{29}$$

where the deformation speed tensor S_{ij} is defined by the relation:

$$S_{ij} = \frac{1}{2}\left(\frac{\partial u_j}{\partial x_i} + \frac{\partial u_i}{\partial x_j}\right) \tag{30}$$

The β^* coefficient is defined by the following relation:

$$\beta^* = \beta_i^*\left[1 + \zeta^* F\left(M_t\right)\right] \tag{31}$$

where:

$$\beta_i^* = \beta_\infty^* \frac{\frac{4}{15} + \left(\frac{\mathrm{Re}_t}{\mathrm{R}_\beta}\right)^4}{1 + \left(\frac{\mathrm{Re}_t}{\mathrm{R}_\beta}\right)^4}, \quad (32)$$

$$\beta_\infty^* = 0.09, \quad (33)$$

$$\mathrm{Re}_t = \frac{\rho k}{\mu \omega}, \quad (34)$$

$$R_\beta = 8 \quad (35)$$

$$\zeta^* = 1.5 \quad (36)$$

and the compressibility function $F(M_t)$ is given by the relation:

$$F(M_t) = \begin{cases} 0 & , M_t \le M_{t0} \\ M_t^2 - M_{t0}^2 & , M_t > M_{t0} \end{cases} \quad (37)$$

where

$$M_t^2 = \frac{2k}{c^2}, \quad (38)$$

$$M_{t0} = 0.25, \quad (39)$$

$$c = \sqrt{\gamma RT} \quad (40)$$

In the transport equation for ρ_ω, G_ω represents the generation of specific turbulent dissipation ω and is obtained from the relation:

$$G_\omega = \frac{\alpha}{\nu_t} G_k = \frac{\alpha}{\frac{\mu_t}{\rho}} G_k \quad (41)$$

It is important to underline the fact that the above definition is different from the one of the standard k-ω turbulence model, yet the α coefficient is defined in the same manner as for the standard k-ω turbulence model:

$$\alpha = \frac{\alpha_\infty}{\alpha^*} \left(\frac{\alpha_0 + \mathrm{Re}_t / \mathrm{R}_\omega}{1 + \mathrm{Re}_t / \mathrm{R}_\omega} \right) \quad (42)$$

where

$$\alpha^* = \alpha_\infty^* \left(\frac{\alpha_0^* + \mathrm{Re}_t / R_k}{1 + \mathrm{Re}_t / R_k} \right), \quad (43)$$

$$R_k = 6, \quad (44)$$

$$R_\omega = 2.95, \quad (45)$$

$$\alpha_0 = \frac{1}{9}, \quad (46)$$

$$\alpha_\infty^* = 1, \quad (47)$$

$$\alpha_0^* = \frac{\beta_i}{3}, \quad (48)$$

$$\beta_i = 0.072 \quad (49)$$

For the standard k-ω turbulence model, a_∞ is defined as a constant ($a_\infty = 0.52$), yet for the SST k-ω turbulence model, a_∞ is defined as a function:

$$\alpha_\infty = F_1 \alpha_{\infty,1} + (1 - F_1) \alpha_{\infty,2} \quad (50)$$

where

$$\alpha_{\infty,1} = \frac{\beta_{i,1}}{\beta_\infty^*} - \frac{\kappa^2}{\sigma_{\omega,1} \sqrt{\beta_\infty^*}}, \quad (51)$$

$$\alpha_{\infty,2} = \frac{\beta_{i,2}}{\beta_\infty^*} - \frac{\kappa^2}{\sigma_{\omega,2} \sqrt{\beta_\infty^*}}, \quad (52)$$

$$\beta_{i,1} = 0.075, \quad (53)$$

$$\beta_{i,2} = 0.0828 \quad (54)$$

$$\kappa = 0.41 \quad (55)$$

The Y_k term represents the dissipation of turbulent kinetic energy k and is defined in the same manner as for the standard k-ω turbulence model, with the main difference being the way in which the f_{β^*} term is evaluated. In the standard k-ω turbulence model, f_{β^*} is defined as a constant, while in the SST k-ω turbulence model, f_{β^*} is defined with the fixed value of 1.

$$Y_k = \rho \beta^* k \omega \quad (56)$$

The Y_ω represents the destruction of the specific turbulent dissipation ω and is defined in the same manner as for the standard k-ω turbulence model. The main difference is the way in which the β_i and f_β terms are evaluated. In the standard k-ω turbulence model, β_i is a constant (0.072) and f_β is a function, while in the SST k-ω turbulence model, f_β is defined with the fixed value of 1. Therefore,

$$Y_\omega = \rho \beta \omega^2 \quad (57)$$

where

$$\beta = \beta_i \left[1 - \frac{\beta_i^*}{\beta_i} \zeta^* F(M_t) \right]. \quad (58)$$

In contrast with the standard k-ω turbulence model where β_i is a constant (0.072), in the SST k-ω turbulence model β_i is a function:

$$\beta_i = F_1\beta_{i,1} + (1-F_1)\beta_{i,2} \quad (59)$$

The SST k-ω turbulence model is based on the standard k-ω and k-ε turbulence models. In order to combine the two turbulence models, the standard k-ω turbulence models were transformed into equations having k and ω as unknown variables, which has led to the introduction of the transversal diffusion D_ω term into the transport equation for $\rho\omega$, defined by the following relation:

$$D_\omega = 2(1-F_1)\rho\sigma_{\omega,2}\frac{1}{\omega}\frac{\partial k}{\partial x_j}\frac{\partial \omega}{\partial x_j} \quad (60)$$

In regard to the limit conditions, at the entrance, the ρk and $\rho\omega$ values have to be imposed, while at the exit there is no need to impose any condition as long as the flow is not inverted. In order to use this turbulence model [15] efficiently, the dimensionless y^+ scale, which represents the distance between the grid nodes and the closest solid wall, should take a value somewhere around that of the integer for calculation cells that have at least one solid frontier. In this case, Menter recommended the following limit conditions:

$$k_P = 0 \quad (61)$$

$$\omega_P = 10\frac{6\nu}{\beta_{i,1}y_P^2} \quad (62)$$

where y_P is the distance to the closest wall. It is important to underline the fact that Wilcox, after considering the wall rugosity, has recommended a different set of relations for ω_P.

3. THE MODEL

It is considered that the Coanda profile type allows the use of axisymmetric flow.

For a numerical simulation of the viscous sublayer, the dimensionless scale y^+ has to be equal or lower than 1, which means that the height of the first cell layer from the solid wall has to be the magnitude of microns for transonic flows.

In order to obtain a grid of a quality as high as possible, the calculations domain has been divided into 14 blocks or 27 blocks (Fig. 3), which has facilitated the achievement of a structured multi-block grid with 12270 or 20655 quadrilateral cells. The extended and restricted domains have been comparatively analyzed for the purpose of studying the limit conditions influence on the results of the numerical simulations.

The flow was presumed to be completely turbulent and the Menter [16] SST k-ω turbulence model was used for calculating the Reynolds (turbulent) tensions, having limit conditions in the wall proximity given by the (61) and (62) relations.

The numerical simulations were achieved by employing the Ansys Fluent 14 code, which is based on the finite volumes method [10], [17], [18], [19], [20]. Upon entering the calculation domain, the total pressure of 1.3 bars and total temperature of 291 K were imposed, the flow was perpendicular on the entrance, the turbulence degree was 5% and the ratio between the turbulent viscosity and the molecular viscosity was 10. At the other domain limit, the only imposed parameters were the static pressure that was equal to the atmospheric pressure.

A resulting acceleration of the air on the upside of the Coanda profile can be observed without any separation, which determined a decrease of static pressure on the upside of the profile, which creates lift. By integrating the static pressure distribution from the Coanda profile, a lift force of 6.47 N is obtained. Unfortunately, when the flow passes from the axial direction to the radial direction, considerable loss of total pressure can be observed, which decreases the Coanda profile resulting lift force.

Upon entering the calculation domain, the following values were imposed:

- absolute total pressure of 1.3 bar,
- total temperature of 291 K,
- flow direction perpendicular on the entrance,
- turbulence degree of 5%,
- ratio between turbulent and molecular viscosity of 10,
- at the other domain limit, the only imposed parameters were the static pressure that was equal to the atmospheric pressure; the other parameters (numerical limit conditions) were extrapolated from inside the calculation domain,
- the walls (solid frontiers) were presumed to be without slip (V_{wall} = 0), without roughness, and the pressure gradient was null (∂p/∂n = 0).

For a numerical simulation of the viscous sublayer, the dimensionless scale y^+ has to be equal or lower than 1, which means that the height of the first cell layer from the solid wall has to be the magnitude of microns for transonic flows.

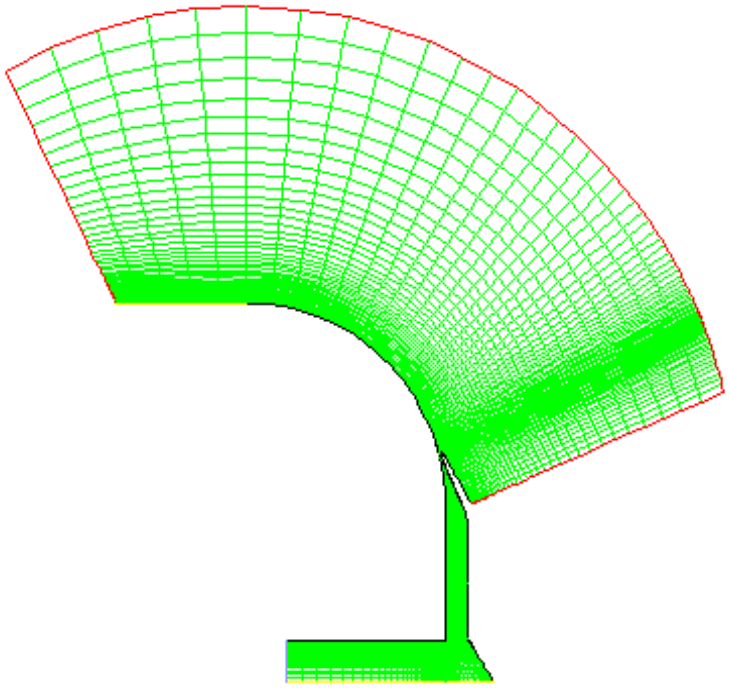

a) Reduced calculation domain

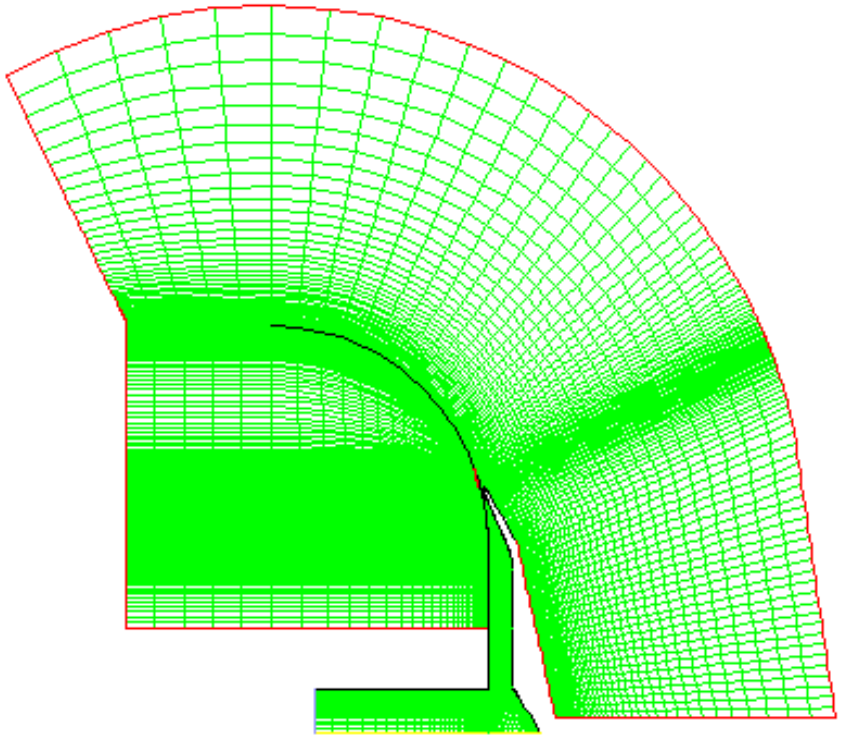

b) Extended calculation domain

Fig. 3. The multiblock structured calculation grid has a) 12 270 cells and b) 20 655 cells; the thickening of the grid in the adjacency of the walls can be observed, for the purpose of a more accurate simulation of the boundary layer

4. RESULTS AND DISCUTION

The authors concluded that the behavior of the system is quite predictable at least for the tested range of the parameters involved (Fig. 4).

The most important results are displayed in figures 5 and 6. A resulting acceleration of the air on the upside of the Coanda profile can be observed (Fig. 5) without any separation, which determined a decrease of the static pressure on the upside of the profile which creates lift. By integrating the static pressure distribution from the Coanda profile, a lift force of 6.47 N is obtained. Unfortunately, when the flow passes from the axial direction to the radial direction, considerable loss of total pressure can be observed, which decreases the Coanda profile resulting lift force.

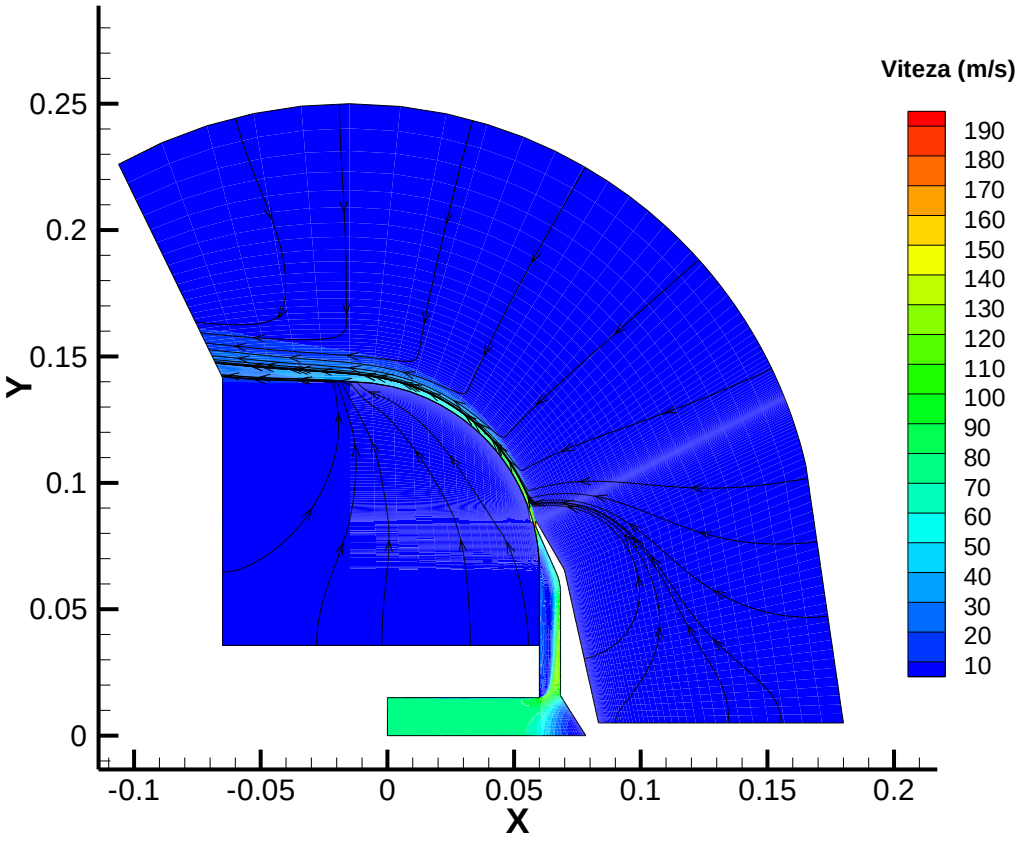

Fig. 4. Flow lines in the adjacency of the Coanda profile upside and in the duct; the fact that the boundary layer remains attached to the upside of the profile and the creation of a powerful vortex in the duct can be observed (extended calculation domain, scale for air velocity in m/s)

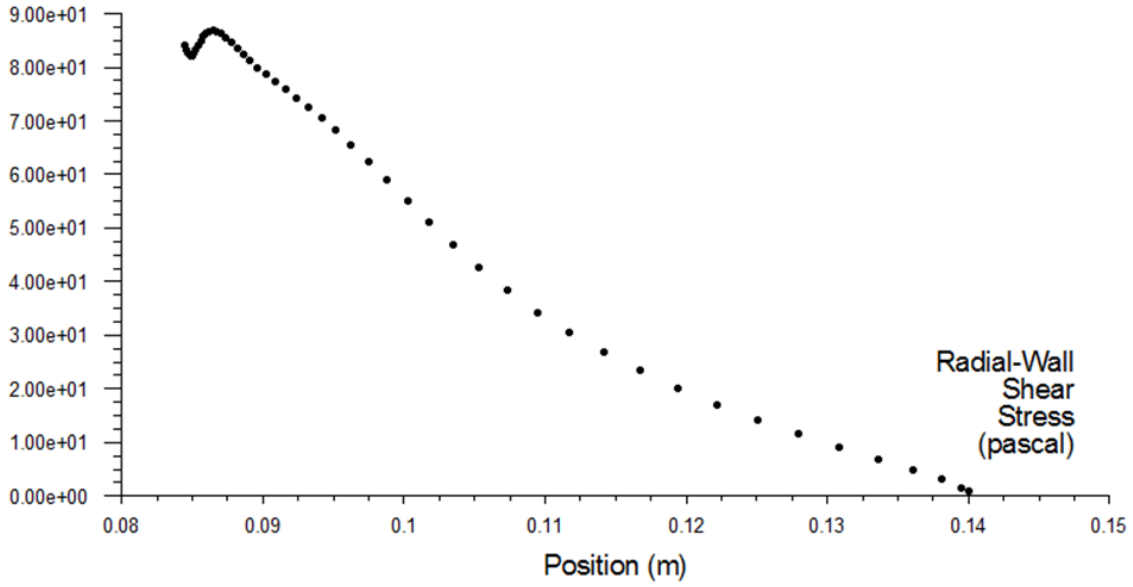

a) Reduced calculation domain

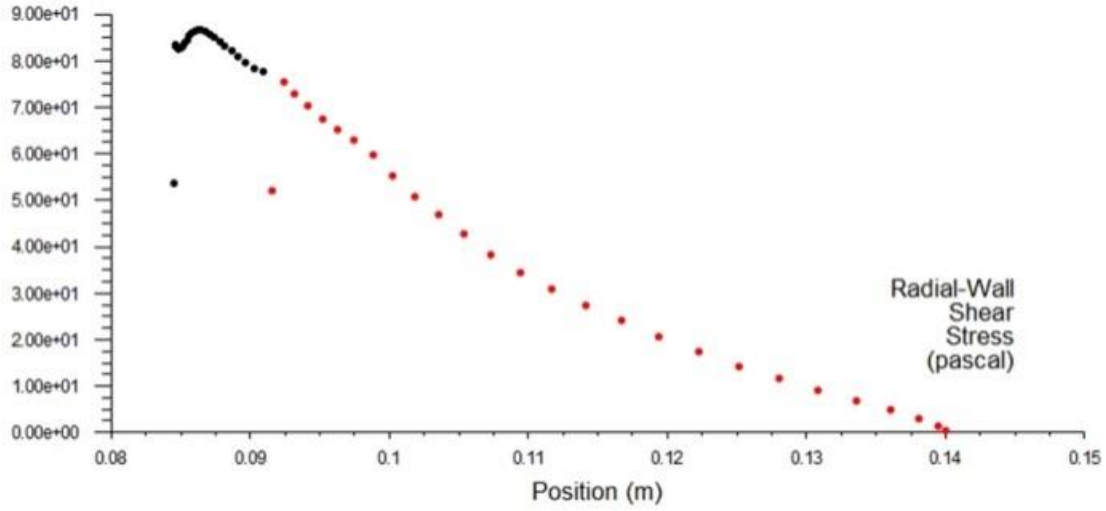

b) Extended calculation domain

Fig. 5. The friction effort on the radial direction for the Coanda profile upside, along the radius; the boundary layer remains attached to the profile

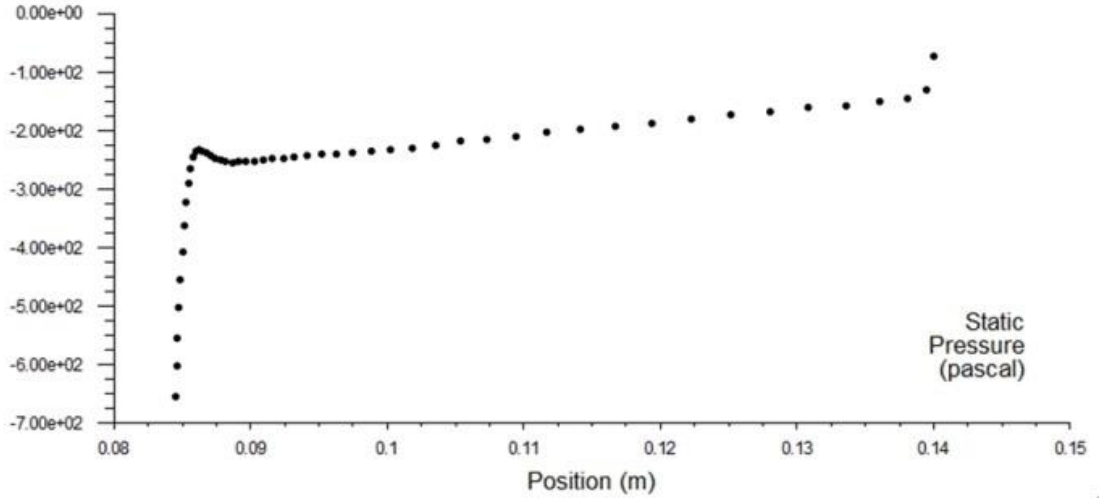

a) Reduced calculation domain

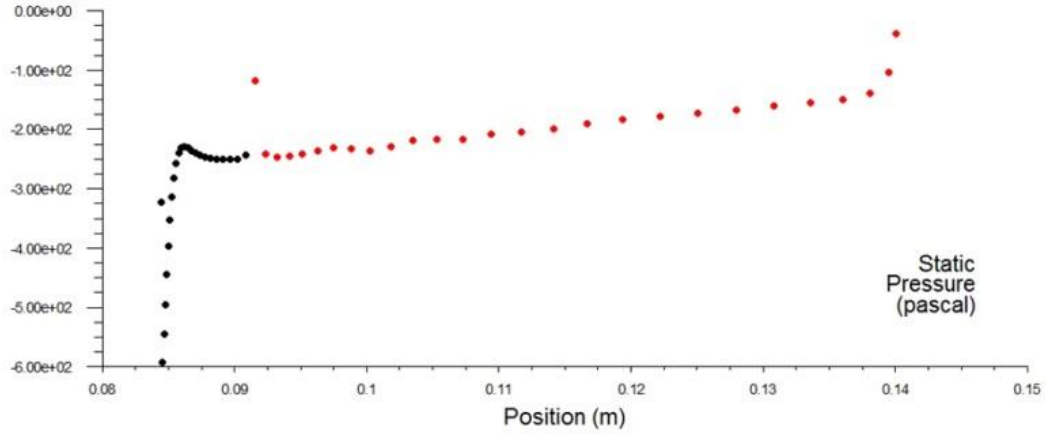

b) Extended calculation domain

Fig. 6. The relative static pressure distribution for the Coanda profile upside, along the radius

5. CONCLUSIONS

The simulation on a Reynolds Averaged Navier-Stokes (RANS) models based on the concept of turbulent viscosity could give valuable information on the behavior of such a system if the appropriate material limit conditions are imposed by the designers. The model proposed by the authors could simulate, with sufficient accuracy, the process of jet attaching on the Coanda profile.

The jet is accelerated across the upside of the Coanda airfoil and, as a consequence of Bernoulli's law, the static pressure drops, for thinner jets and higher velocities, the jet does not detach from the surface of the Coanda airfoil.

REFERENCES

1. C. Donaldson and H. Rosembaum, Calculation of the turbulent shear flows through closure of the Reynolds equations by invariant modeling, Rept. No. 127, Aero. Res. Assoc., Priceton, 1968.
2. D. Charbonnier, Développement d'un modèle de tensions déterministes instationnaires adapté à la simulation de turbomachines multi-étagées, Thèse de doctorat, École Centrale de Lyon, 2004.
3. D. Choudhury, Introduction to the renormalization group method and turbulence modeling, Technical Memorandum TM-107, Fluent Inc., 1993.
4. G. Bălan, S. G. Constantinescu, B. Ciobanu, The Coandă Vtol-Uav Aeromechanical Aspects, the 13th Intern. Conf. AFASES 2011, Brasov, pp. 1205-1210, May 2011.
5. F. Harlow and P. Nakayama, Turbulent transport equation, *The Physics of Fluids*, Vol. 10, pp. 2323-2332, 1967.
6. J. Dacles-Mariani, G. G. Zilliac, J. S. Chow and P. Bradshaw, Numerical/experimental study of a wingtip vortex in the near field, *AIAA Journal*, Vol. 33, No. 9, pp. 1561-1568, 1995.
7. B. Davidov, On the statistical dynamics of an incompressible turbulent fluid, Dokl. AN SSSR, Vol. 47, 1961.

8. F. R. Menter, Two-equation eddy-viscosity turbulence models for engineering applications, *AIAA Journal*, vol. 32, No. 8, pp. 1598-1605, August 1994.
9. W. Rodi, Turbulence models and their applications in hydraulics, Technical report, 2nd Edition, *International Association for Hydraulic Research– Publication*, Delft, 1984.
10. W. Jones and B. Launder, The prediction of laminarization with two-equation model of turbulence, *International Journal of Heat and Mass Transfer*, Vol. 15, Issue 2, pp. 301-314, 1972.
11. M. L. Shur, M. K. Strelets, A. K. Travin and P. R. Spalart, Turbulence modeling in rotating and curved channels: assessing the Spalart-Shur correction, *AIAA Journal*, Vol. 38, No. 5, pp. 784-792, 2000.
12. D. C. Wilcox, Comparison of two-equation turbulence models for boundary layers with pressure gradient, AIAA Journal, Vol. 31, No. 8, pp. 1414-1421, 1993.
13. P. Spalart and S. Allmaras, A one-equation turbulence model for aerodynamic flows, *La Recherche Aérospatiale*, No. 1, pp. 5-21, 1994.
14. D. Spalding, The k-ε model of turbulence, Technical Report TM/TN/A/16, Imperial College, Dep. Mech. Eng., 1971.
15. G. Fetea, M. L. Niculescu, V. Silivestru, B. Gherman G. Vizitiu and C. Stănică, Aerodynamic analysis of a centrifugal blower impeller, *Romanian Conference of Ansys and Fluent*, Sinaia, 2008.
16. Ch. Hirsch, *Numerical Computation of Internal and External Flow, Volume 2: Computational Methods for Inviscid and Viscous Flows*, John Wiley and Sons, New York, 1990.
17. V. N. Constantinescu, S. Dănăilă and S. Găletuşe, *Dinamica fluidelor în regim turbulent* (in Romanian), Editura Academiei Române, Bucureşti, 2008.
18. A. Kolmogorov, Equation of turbulent motion of an incompressible fluid, *Izv. Akad. Nauk. SSR*, No. 1-2, pp. 56-58, 1942.
19. D. C. Wilcox, Comparison of two-equation turbulence models for boundary layers with pressure gradient, *AIAA Journal*, Vol. 31, No. 8, pp. 1414-1421, 1993.
20. D. C. Wilcox, Turbulence Modeling for CFD, 2nd edition, DCW Industries, Inc., La Canada, California, 1998.